

1 **Mycobacterial OtsA structures unveil substrate preference mechanism and**
2 **allosteric regulation by 2-oxoglutarate and 2-phosphoglycerate**

3

4

5 **Vítor Mendes^{1*}, Marta Acebrón-García-de-Eulate¹, Nupur Verma¹, Michal**
6 **Blaszczyk¹, Márcio V. B. Dias^{2,3} and Tom L. Blundell^{1*}**

7

8 1 - Department of Biochemistry, University of Cambridge, Cambridge CB21GA, UK.

9 2 - Department of Microbiology, Institute of Biomedical Science, University of São
10 Paulo, São Paulo, Brazil.

11 3 – Department of Chemistry, University of Warwick, Coventry CV4 7EQ, UK.

12 *Corresponding authors

13 Tom L. Blundell

14 Address: Department of Biochemistry, University of Cambridge, 80 Tennis Court Road,
15 CB2 1GA Cambridge, UK.

16 Phone: +441223333628

17 Email: tom@cryst.bioc.cam.ac.uk

18 Vitor Mendes

19 Address: Department of Biochemistry, University of Cambridge, 80 Tennis Court Road,
20 CB2 1GA Cambridge, UK.

21 Phone: +441223766028

22 Email: vgm23@cam.ac.uk

23

24

25

26

27 **Abstract**

28 Trehalose is an essential disaccharide for mycobacteria and a key constituent of several
29 cell wall glycolipids with fundamental roles in pathogenesis. Mycobacteria possess two
30 pathways for trehalose biosynthesis. However, only the OtsAB pathway was found to be
31 essential in *M. tuberculosis*, with marked growth and virulence defects of OtsA mutants
32 and strict essentiality of OtsB2. Herein, we report the first mycobacterial OtsA structures
33 from *M. thermoresistibile* in both apo and ligand-bound forms. Structural information
34 reveals three key residues in the mechanism of substrate preference that were further
35 confirmed by site-directed mutagenesis. Additionally, we identify 2-oxoglutarate and 2-
36 phosphoglycerate as allosteric regulators of OtsA. The structural analysis in this work
37 strongly contributed to define the mechanisms for feedback inhibition, show different
38 conformational states of the enzyme and map a new allosteric site.

39

40

41

42

43

44

45

46

47

48

49

50

51 **Introduction**

52

53 Trehalose is a non-reducing disaccharide, formed by α -(1-1) linked glucoses, with a wide
54 distribution in nature and present in all three domains of life (1). This remarkably
55 widespread sugar performs multiple roles in a wide variety of organisms and it can also
56 fulfil different roles within the same organism. Trehalose has been considered a
57 compatible solute, conferring protection to proteins, DNA, membranes and whole cells
58 from thermal shock, osmotic shock, freezing, ionizing radiation, oxidative stress and
59 desiccation (1-9). This disaccharide, which can further function as a carbon and energy
60 reserve molecule (1, 10-12), was also recently related to pathogenicity of *Pseudomonas*
61 *aeruginosa* in plants (13). It additionally plays fundamental signaling roles in plants in
62 the phosphorylated form (trehalose-6-phosphate) where it regulates sucrose metabolism
63 and flowering (1, 14-16) and in yeast where it regulates gluconeogenesis and glycolysis
64 (17, 18). Trehalose was further shown to be an autophagy inducer, both in plants and in
65 mammals, with potential biotechnological and clinical implications (19, 20).

66 In mycobacteria, trehalose is also an essential component of mycolic acids and other cell
67 wall glycolipids, which are major protagonists in *Mycobacterium tuberculosis*
68 pathogenesis (1), the causative agent of the widespread infectious disease tuberculosis. In
69 these organisms, trehalose was further identified as a key signaling molecule of cell-
70 envelope stress playing a role as an activator of the iniBAC operon, which is induced
71 when mycobacteria are exposed to the first line drug isoniazid (21).

72 All mycobacterial species, with a few exceptions, possess two pathways to synthesize
73 trehalose, the OtsAB and the TreYZ pathway (1). The OtsAB pathway is the most widely
74 distributed trehalose biosynthesis pathway, present in bacteria, archaea and eukaryotes
75 (22, 23). In this pathway, which is conserved and essential in mycobacteria, trehalose is

76 synthesized in a two-step process involving OtsA and OtsB2 enzymes. *M. tuberculosis*
77 mutants showed that the OtsAB pathway was not only the dominant route for trehalose
78 biosynthesis in this pathogen but also required for growth both *in vitro* and in a mouse
79 infection model, with marked growth and virulence defects of OtsA mutants (24) and
80 strict essentiality of OtsB2 due to the toxic effect of trehalose-6-phosphate (T6P)
81 accumulation (24, 25).

82 OtsA, a glycosyltransferase that belongs to the GT20 family of the CAZY classification
83 (www.cazy.org), uses the α anomer of glucose-6-phosphate (G6P) as acceptor and NDP-
84 glucose as the donor to synthesize T6P, with net retention of the anomeric configuration
85 of the donor substrate (26, 27). Interestingly, OtsAs from different organisms show
86 different donor preferences as shown by kinetic studies and X-ray crystal structures, but
87 the reasons behind these preferences are poorly understood (27-32). Recently, different
88 roles were identified for OtsA beyond its enzymatic activity. OtsA was reported to act as
89 an osmotic stress sensor and morphogenetic protein that can regulate the switch to
90 myceloid growth in *Arthrobacter sp.* strain A3, a pleomorphic soil dwelling
91 actinobacteria (33).

92 In this work we have purified, crystallized and solved the structure of *Mycobacterium*
93 *thermoresistibile* OtsA (*MtrOtsA*). To gain further insight into mycobacterial OtsA, we
94 have obtained structures with substrates, product and pathway product that offer insight
95 for mechanisms of ADP-glucose preference and feedback inhibition by trehalose. We
96 further performed structure-guided point mutations of key residues of the active site and
97 characterized the mutants showing that three mutations are enough to change the donor
98 substrate preference to UDP-glucose. Importantly with these structures, we have also
99 identified a new allosteric site and novel allosteric regulators of this enzyme that link
100 glycolytic and TCA cycle metabolites to the regulation of trehalose synthesis.

101 **Results**

102

103 **Overall structure**

104 The structure of *MtrOtsA* in apo form was solved by molecular replacement, using *E. coli*
105 OtsA structure (PDB code: 1UQU) as the search model. Data collection and refinement
106 statistics are summarized in (Table S1). *MtrOtsA* is composed of two Rossmann-fold
107 domains with a deep catalytic site at their interface, in an arrangement typical of GT-B
108 glycosyltransferases as described previously for other organisms (27-29). The apo protein
109 crystallized in the $I4_122$ space group, with one protomer per asymmetric unit, and
110 diffracted to ~ 1.8 Å resolution. The N-terminal domain is formed by a core of 7 parallel
111 β -strands flanked on both sides by an antiparallel β -strand and surrounded by 8 α -helixes,
112 one of which is composed of the final C-terminal residues (Fig. 1A). The C-terminal
113 domain contains 6 parallel β -strands associated with 9 α -helixes with the last one
114 undergoing a kink and extending to the N-terminal domain, characteristic of the GT-B
115 fold glycosyltransferases (Fig 1A). Analysis of the B-factor distribution shows that the
116 N-terminal domain has the highest values for atomic temperature factors, suggesting that
117 this domain is more dynamic, which is consistent with the large movements of α -1 during
118 catalytic activity.

119 *MtrOtsA* forms a tetramer in solution, as previously observed for *M. tuberculosis* OtsA.
120 This tetrameric form is also observed in all the crystal structures reported herein (Fig 1B).
121 The amino acids involved in the tetramer interfaces are not conserved beyond
122 mycobacteria and related species (Fig S1), suggesting that OtsA might have a different
123 molecular assembly in different species. Indeed in *Escherichia coli* both tetrameric and
124 dimeric forms were reported (27) and in *Streptomyces venezuelae*, *Aspergillus fumigatus*
125 and *Candida albicans* only the dimeric form was observed (28, 29). However, in

126 mycobacteria and closely related organisms the tetramer interfaces are highly conserved,
127 suggesting a tetrameric assembly of OtsA in all of these organisms (Supplementary Fig
128 S1).

129

130 **Catalytic site**

131 OtsA, is a glycosyltransferase that uses the α anomer of G6P as acceptor and NDP-
132 glucose as the donor to synthesize T6P. The *Mtr*OtsA catalytic site is located between the
133 two Rossmann-fold domains in a large and deep cavity. Structures with donor substrates
134 were determined by soaking the apo form crystals with ADP-glucose and GDP-glucose
135 (Fig 2). The donor substrates interact primarily with the C-terminal domain through the
136 side chains of the highly conserved Arg286, Lys 291, Asp385, Glu393 and with the side
137 chain of Arg365 (Fig 2), which is conserved in all mycobacteria and closely related
138 species but less conserved outside this group (Fig S1). Backbone interactions with the
139 absolutely conserved residues Gly386, Met387 and Leu389 amine groups are also
140 observed. N-terminal domain interactions with the donor substrate are only observed for
141 His168 when the active site is in an open conformation (Fig 2). To obtain a structure with
142 the acceptor substrate, we co-crystallized OtsA in the presence of 5 mM ADP and G6P.
143 As G6P binds to the protein in the presence of a donor substrate or its nucleotide, the
144 active site adopts to a closed conformation (Fig 3A). The OtsA:ADP:G6P ternary
145 complex crystallized in the P6₂22 space group, with one protomer per asymmetric unit,
146 and the crystals diffracted up to ~1.7 Å resolution. In this closed conformation new
147 interactions with the donor substrate are formed with the side chain of Thr42 and the
148 Gly39 peptide-NH function (Fig 3). Due to the absolute conserved nature of Gly39 and
149 the contact it forms with the glucose-bound phosphate, this residue is highly likely to be
150 mechanistically involved in the catalytic activity (27).

151 The acceptor substrate interacts with the highly conserved residues Arg18, Tyr90,
152 Asp144 and Gln146 of the N-terminal domain and with only a single residue of the C-
153 terminal domain, Arg324 (Fig 3B). The residues involved in acceptor substrate
154 interaction are highly conserved in all species (Fig S1). As described for *E. coli* OtsA
155 (27), the OtsA:ADP:G6P ternary structure shows the catalytic site in a closed
156 conformation that substantially differs from the apo form, with α -helix 1 and the Arg35-
157 Gly39 loop region moving up to ~ 12 Å (Fig 3A).

158

159 **Properties of *M. thermoresistibile* OtsA.**

160 *Mtr*OtsA uses ADP-glucose, UDP-glucose and GDP-glucose as glucose donors with
161 decreasing efficiency (Table 1) and G6P as the only acceptor, in accordance to what was
162 reported before for *M. tuberculosis* OtsA (32, 34). The kinetic parameters for *Mtr*OtsA
163 were obtained and are reported in (Table 1) and (Fig. S2) with K_m values for preferred
164 donor substrate (ADP-Glucose) of 0.25 ± 0.02 mM and for the acceptor (G6P) of $3.3 \pm$
165 0.1 mM. The K_m for GDP-glucose of 0.29 ± 0.02 mM was in the same range as the one
166 obtained for ADP-glucose, however the turnover was 5 fold lower (Table 1). For UDP-
167 glucose, the enzyme showed a ~ 7 fold higher K_m of 1.7 ± 0.1 mM than the one obtained
168 for ADP-glucose (Table 1).

169 The preference of ADP-glucose over the other glucose donors was further confirmed by
170 isothermal titration calorimetry (ITC). The binding affinity of substrate donors could only
171 be determined for ADP-glucose in the tested conditions with an observable K_d of $27.17 \pm$
172 2.66 μ M (Fig S3). Other glucose donors analysed (GDP-glucose and UDP-glucose) had
173 no observable heat of binding and the same was observed for G6P. The lack of heat of
174 binding for GDP- and UDP-glucose is most likely due to their reduced affinity. For G6P
175 case, it reflects a necessity of previous binding of the donor substrate.

176

177 **Donor substrate preference is largely mediated by three residues**

178 OtsAs from different organisms have been shown to have different donor substrate
179 preferences, while being capable of using several nucleotide donors (29, 32, 35, 36),
180 which is reflected in lower conservation of the donor substrate interacting residues (Fig
181 S1). Preference for ADP-glucose as the donor substrate in *Mtr*OtsA is conferred by
182 interactions with the deeply buried adenine moiety (Fig 4A). The carbonyl groups of
183 Leu319 and Arg361 interact with the primary amine, and the amide group of Val363
184 interacts with N1 of the adenine moiety (Fig 4A). A highly coordinated water is also
185 interacting with the primary amine of the adenine moiety and the carbonyl groups of
186 Ala320, Leu359 and Arg361. The guanine moiety of GDP-glucose cannot occupy the
187 same deeply buried pocket as the adenine because its primary amine group would
188 sterically clash with Val363 carbonyl group (Fig 4B). It thus binds to OtsA more weakly
189 than ADP-glucose explaining the substrate preference and consequently the lack of
190 observable heat of binding in the tested ITC conditions. A binary complex structure with
191 OtsA and UDP-glucose was also obtained but the electron density was only observed for
192 glucose and the two phosphates (not shown) indicating a reduced preference for this
193 substrate as confirmed by enzymatic and biophysical data. Comparing mycobacterial
194 OtsAs with *E. coli*, we hypothesised that the ADP preference was mediated by the
195 substitution of an isoleucine (Ile295 in *E. coli*) for a leucine (Leu319 in *M.*
196 *thermoresistibile*) that allows the primary amine of the adenine moiety to occupy a buried
197 position interacting with the carbonyl group of Leu319 (Fig 4C) that no other nucleotide
198 activated donor can occupy. However, given the residue differences between the two
199 enzymes it is likely that other residues could also play a role. To improve the selection of
200 residues to mutate we employed a computational approach by using a mCSM-lig (37), a

201 software developed by our group that predicts the effects of mutations on binding affinity.
202 The software predicted several that residues within 4.5 Å of the adenine moiety have a
203 destabilizing effect on the interaction with the ligand if mutated to the *E. coli* OtsA
204 equivalent (Table S2). Combining this information with structural analysis we selected
205 three mutations predicted to be destabilizing; Val363Phe, Leu319Ile and Glu367Leu, the
206 latter being a long distance mutation that we hypothesised would have a strong effect on
207 ligand binding.

208 To confirm our hypothesis, we generated several *Mtr*OtsA mutants (Leu319Ile,
209 Val363Phe, Leu319Ile-Glu367Leu and a triple mutant) and we obtained kinetic
210 properties for all of them (Table 1). As we predicted the mutant Leu319Ile showed a ~3
211 fold increase in the K_m for ADP-glucose whereas, K_m was similar for GDP-glucose and
212 UDP-glucose when compared to the wild type. Even though GDP-glucose now showed
213 the best K_m among the three different donors, the catalytic efficiency and turnover rate
214 was still higher for ADP-glucose (Table 1). A complete reversal of the donor substrate
215 preference for UDP-glucose was obtained only with a combination of the three mutations
216 (Table 1). The triple mutant showed a ~5 fold increase in ADP-glucose K_m and a reduction
217 for the UDP-glucose K_m by more than 3 fold (Table 1). The catalytic efficiency was also
218 completely reversed for ADP- and UDP-glucose between the wild-type and the triple
219 mutant (Table 1). Although Leu319Ile showed the largest contribution for ADP-glucose
220 K_m increase, Val363Phe and Glu367Leu were also determinant for the reversal to UDP-
221 Glucose preference (Table 1). This can be explained by the fact that the phenylalanine
222 substitution at position 363 forces the loop between β -14 and α -14 to move towards the
223 nucleotide binding site (Fig 4C), thus establishing stronger interactions with a pyrimidine
224 nucleotide and clashing with purine ones. This effect is also observed for both ADP- and
225 GDP-glucose, with a ~2.5 fold increase in K_m when compared to the wild type. The

226 leucine substitution at position 367 further helps in this move since the hydrogen bonds
227 between the side chains of Arg266 and Glu367 are no longer present and α -14 is repelled
228 from Arg266 due to the Leu side chain (Fig 4C).

229

230 **Feedback inhibition**

231 We soaked both trehalose and T6P into apo OtsA crystals and solved structures with both
232 ligands (Fig 4D and 4E). In both structures OtsA active site assumes an open
233 conformation and two compounds superpose almost perfectly at active site, recapitulating
234 all of the interactions for the donor glucose and also interacting with His199 and Arg286,
235 the latter a residue that interacts with the phosphates of the donor substrate (Fig 4D and
236 4E). The structure with T6P further shows the phosphate group of the product occupying
237 a similar position to the phosphate group of G6P, interacting with the side chains of
238 Tyr90, Gln146, Arg324 and Tyr145 a residue that does not interact with G6P (Fig 4E).
239 Interestingly the buffer present in the crystallization condition (CHES) is observed in both
240 trehalose and trehalose-6-phosphate bound structures, occupying the site of the nucleotide
241 donor with the sulphate group binding in a phosphate site and interacting with hydroxyl
242 groups from both glucose units of trehalose (Fig 4D and 4E).

243 After obtaining these structures, it was expected to observe some degree of feedback
244 inhibition of OtsA by both trehalose and T6P. Both trehalose-6-phosphate and trehalose
245 inhibited the enzyme, but the effect of trehalose was more pronounced with ~40%
246 inhibition at 10 mM while for trehalose-6-phosphate a maximum inhibition of ~25% was
247 reached at the same concentration (Fig S4). These results show that under physiological
248 conditions OtsA is regulated by trehalose, the final product of the pathway which is highly
249 abundant inside mycobacterial cells, but not by T6P which could not be detected in *M.*
250 *tuberculosis* cell extracts under physiological conditions (25).

251

252 **Identification of an allosteric site in *M. thermoresistible* OtsA**

253 Trehalose is a multipurpose molecule that is abundant in mycobacteria. It can function
254 not only as an energy reserve and as structural component of cell wall glycolipids, but
255 can also lead to the synthesis of glycogen through the TreS-Mak-GlgE pathway and be
256 directly synthesised from glycogen from the TreX-TreY-TreZ pathway. It is therefore
257 likely that trehalose synthesis through the OtsA-B pathway is under strong regulation.

258 In all the crystallization conditions that contained CHES, we could observe this
259 compound in the crystal structures occupying a pocket formed by the contact interface of
260 2 OtsA protomers in the tetrameric assembly (Fig 5). The CHES sulphate group directly
261 interacts with the side chains of Arg384 of protomer A and Arg213 of protomer B,
262 forming hydrogen bonds with both, but also hydrophobic hydrogen- π interactions with
263 Phe410 of protomer A (Fig 5). The residues composing this site are completely conserved
264 in mycobacterial and closely related species that are likely to harbour OtsA tetramers but
265 not on others species known to have other oligomeric forms (Fig S1).

266 Arg384 sits in a loop that forms extensive contacts with the donor substrate through
267 Asp385, Gly386, Met387 and Leu389 (Fig 2). Ligands interacting with the side chain of
268 Arg384 could therefore have an impact on the activity of the enzyme making this site a
269 prime candidate for allosteric regulation.

270 While CHES had no discernible impact on OtsA activity in the tested concentrations, it
271 was reported before that F6P acted as an allosteric regulator of *M. tuberculosis* OtsA (34),
272 and the same was reported for yeast OtsA-B complex (38). We have tested *Mtr*OtsA in
273 the same conditions as those reported by Diez and colleagues (34), and could not detect
274 any effect of F6P for *Mtr*OtsA. Although we did not observe any effect of F6P on enzyme
275 activity for *Mtr*OtsAs, we nevertheless attempted to soak this compound in both apo form

276 and OtsA:ADP:G6P ternary complex crystals, and also co-crystallize it in the presence
277 and absence of ADP and G6P, all in CHES free conditions. None of these conditions
278 provided a structure in which F6P occupied an allosteric site. We could however observe
279 F6P when co-crystallized together with ADP, bound to the acceptor substrate site, with
280 OtsA presenting the active site in a closed conformation (Fig S5).

281 OtsA was found to interact with a multitude of proteins in a large-scale proteomics study
282 (39), including enolase that catalyses the penultimate step of glycolysis. In our search for
283 an allosteric regulator we, therefore, decided to test several glycolytic metabolites
284 glucose-1-phosphate (G1P), fructose-1,6-biphosphate (F16BP), 3-phosphoglycerate
285 (3PG), the enolase substrate 2-phosphoglyceric acid (2PG) and product
286 phosphoenolpyruvate (PEP), but also the master metabolic regulators cAMP and 2-
287 oxoglutarate (2OG) (40), and assess their impact in OtsA activity.

288 From the several compounds tested only 2OG and 2PG showed clear inhibition of OtsA
289 activity with IC_{50} of 1.8 mM and 2.3 mM respectively (Table 2) and (Fig 5C). To assess
290 whether they could be acting allosterically on *MtrOtsA* and binding to the site identified
291 by CHES we performed two mutations on the arginines that interacted with CHES
292 (Arg213Glu and Arg384Glu) and tested the two mutants activity in the presence of 2OG
293 and 2PG. The results show that the Arg213Glu mutation abolished the strong response of
294 the protein to 2OG while there was a ~5 fold increase in 2PG IC_{50} to 12 mM. For the
295 Arg384Glu mutant 2OG becomes unexpectedly becomes a strong activator with an EC_{50}
296 of 0.7 mM while 2PG has no effect (Table 2).

297

298 **Discussion**

299 Trehalose, an essential disaccharide in mycobacteria, is one of the critical components of
300 the cell wall. The OtsA-B pathway is an essential source of trehalose for these organisms

301 with knockouts of this pathway being growth defective or non-viable (24, 25). Here we
302 reveal the first mycobacterial OtsA structure. The overall structure of *M. thermoresistibile*
303 OtsA is similar to the reported structures of *E. coli*, *S. venezuelae* and *Paraburkholderia*
304 *xenovorans* OtsAs despite relatively low sequence identity (30-35%). Remarkably, OtsAs
305 have also a highly similar fold to the pseudo-glycosyltransferases VldE and ValL
306 involved in validamycin A synthesis, a potent antifungal agent (41, 42).
307 Nevertheless, there are substantial differences in the oligomeric organization of bacterial
308 OtsAs, with tetrameric, dimeric and protomeric forms reported. While mycobacteria and
309 related species present conservation of interfaces showing that the observed tetrameric
310 form for *Mtr*OtsA is present in all these organisms, beyond this group such conservation
311 is absent, which is consistent with other oligomeric states (Figure S1).
312 The structures obtained in this work allow us to explain how mycobacterial OtsA
313 preference for ADP-glucose, is conferred by Leu319 which creates a cavity to
314 accommodate the primary amine of the adenine moiety allowing it to interact with Leu319
315 and Arg361 carbonyl groups. It is further mediated by Val363 carbonyl group that does
316 not allow GDP-glucose to occupy the same position and Glu367. Mutating these three
317 residues to the *E. coli* OtsA equivalents completely changed the preference to UDP-
318 glucose, the preferred *E. coli* OtsA donor substrate. Both Leu319 and Glu367 are highly
319 conserved in all mycobacterial and closely related species analysed but not beyond this
320 group, while Val363 can be replaced by other small hydrophobic amino acids such as
321 alanine and isoleucine in other mycobacterial species and closely related species (Figure
322 S1). However, outside this group Val363 is replaced by bulkier residues such as tyrosine
323 and phenylalanine (Figure S1). These differences are suggestive of alternative donor
324 substrate preferences for organisms outside the sub-order *Corynebacterineae*.

325 Trehalose is not only abundant inside the mycobacterial cell but also involved in a cycle
326 that links it to the synthesis and degradation of glycogen (43). We have shown that OtsA
327 is feedback inhibited by trehalose but not by T6P even though the structures obtained
328 show that both compounds form extensive interactions with OtsA. However, given that
329 these two structures were obtained by soaking apo form crystals with high concentrations
330 of trehalose and T6P, and that CHES is also observed at the active site interacting with
331 both compounds, it is possible that these two structures do not entirely reflect their natural
332 interactions with the enzyme. The toxic accumulation of T6P in OtsB2 knockout mutants
333 (25) can be explained by these results since OtsA shows very low sensitivity to T6P.
334 Furthermore trehalose levels are reduced in the mutant (25) further contributing to an
335 increase in OtsA activity leading to higher T6P production.

336 Regulation of OtsA by phosphorylation and methylation has been observed for yeast
337 trehalose-6-phosphate synthase complex (44, 45) and phosphorylation of *E. coli* OtsA has
338 also been reported (46) in two residues close to the active site. Even though only one of
339 the residues is conserved in mycobacteria (Ser323 for *Mtr*OtsA), phosphorylation of this
340 residue would most likely lead to inactivation of the enzyme due to the location close to
341 the acceptor binding site (Fig S6). Interestingly this residue is highly conserved in all
342 sequences analysed with a single exception where it is substituted by a threonine (Figure
343 S1), suggesting that phosphorylation of this residue might be a common regulatory
344 mechanism of OtsA activity.

345 Allosteric regulation was reported for both *M. tuberculosis* OtsA and yeast trehalose
346 phosphate synthase complex, mediated by F6P (34, 38). The structure obtained with F6P
347 shows this compound occupying the donor site, in the presence of ADP, with the enzyme
348 adopting a closed conformation. Nevertheless, OtsA could only use G6P as an acceptor
349 and F6P showed no effect in the enzyme activity, indicating that the presence of F6P in

350 the acceptor site was forced by the high concentration used for co-crystallization (5mM).
351 The observed differences in regulation by F6P between mycobacterial enzymes are
352 difficult to reconcile since the allosteric site is highly conserved in mycobacterial OtsAs
353 and closely related species (Fig S1).
354 *Mtr*OtsA is allosteric regulated by 2PG, the substrate of enolase, a glycolytic enzyme,
355 and 2OG a master metabolic regulator that sits at the interface of carbon and nitrogen
356 metabolism. The observed effect is within relevant physiological concentrations for both
357 compounds (47, 48).
358 The effect of 2PG on OtsA and the reported interaction with enolase suggests an interplay
359 between these two enzymes that would be interesting to explore further on the enolase
360 side. Enolase is a multifunctional protein involved in a variety of cellular processes,
361 beyond its enzymatic activity, that include response to oxidative and thermal stress (49),
362 and is further involved in the RNA degradosome activity, by regulating RNA stability in
363 response to stress (50, 51). Given that trehalose is a known chemical chaperone and
364 compatible solute (1), the association between enolase and OtsA, through the effect of
365 2PG in OtsA activity and the reported interaction between the two enzymes, points to
366 further regulation to stress response that would be interesting to explore further on the
367 enolase side.
368 2OG is a molecule that sits at the interface of carbon and nitrogen metabolism and that
369 has been shown to regulate many different pathways (40). The role of trehalose as an
370 energy reserve molecule (1) and its relationship with synthesis and degradation of
371 glycogen (52) points to a mechanism in which 2OG influences the synthesis of these two
372 compounds through regulation of OtsA activity that deserves to be further explored.
373 We have shown that OtsA can be allosteric inhibited, however a single mutation at the
374 allosteric site changed the behaviour of 2OG, but not 2PG, from an inhibitor to an

375 activator. This hints at the possible existence of allosteric activators of OtsA to be
376 discovered.

377 The conservation of allosteric site residues and oligomeric assembly in the sub-order
378 *Corynebacterineae* but not outside, suggests that allosteric regulation of OtsA through
379 this site might be limited to this group of organisms. The results of this work are a
380 significant step forward in understanding the regulation of trehalose synthesis in
381 mycobacteria the structural reasons behind substrate preference, and provide new
382 important insight into this enzyme.

383

384 **Methods**

385

386 **Bacterial strains and cloning.**

387 *M. thermoresistibile* (DSM 44167) *otsA* gene was amplified from chromosomal DNA
388 obtained from the Deutsch Sammlung von Mikroorganismen und Zellkulturen GmbH
389 (DSMZ, Braunschweig, Germany). Primers were designed based on the sequence
390 available in NCBI database and the gene was cloned between the BamHI and HindIII
391 sites in pET28a vector (Novagen), modified with an N-terminal 6xHis-SUMO tag. The
392 resulting plasmid was confirmed by DNA sequencing and transformed into *E. coli*
393 BL21(DE3) strain (Invitrogen). Six *MtrOtsA* mutants (Arg213Glu, Leu319Ile,
394 Val363Phe, Arg384Glu, Leu319Ile-Glu367Leu and Leu319Ile-Val363Phe-Glu367Leu)
395 were also constructed by site-specific mutagenesis, sequenced and transformed into *E.*
396 *coli* BL21(DE3) strain. Primers used in this work are listed in table S3.

397

398 **Recombinant expression and protein purification**

399 Transformed *E. coli* BL21(DE3) cells were grown to mid-exponential growth phase
400 ($OD_{610} = 0.6$) in LB media (Invitrogen) containing 30 mg L⁻¹ kanamycin at 37 °C.
401 Isopropyl β-D-1-thiogalactopyranoside (IPTG) was then added at a final concentration
402 of 0.5 mM to induce gene expression and the temperature was lowered to 18 °C. Cells
403 were harvested 18 h-20 h later by centrifugation and re-suspended in 20 mM TRIS pH
404 7.5, 500 mM NaCl and 20 mM Imidazole with protease inhibitor tablets (Roche), DNaseI
405 and 5 mM MgCl₂. Cells were lysed by sonication and cell lysate was centrifuged at 27000
406 g for 30 min to remove cell debris.

407 Recombinant *MtrOtsA* was purified with a HiTrap IMAC Sepharose FF column (GE-
408 Healthcare), equilibrated with 20 mM TRIS pH 7.5, 500 mM NaCl and 20 mM Imidazole.
409 Elution was performed in the same buffer, but with 500 mM Imidazole. Imidazole was
410 removed with a desalting column and SUMO tag was cleaved overnight at 4 °C by adding
411 Ulp1 protease at 1:100 ratio in 20 mM TRIS pH 7.5, 500 mM NaCl. SUMO tag, Ulp1
412 protease and uncleaved SUMO-OtsA were removed with a HiTrap IMAC Sepharose FF
413 column (GE-Healthcare), equilibrated with 20 mM TRIS pH 7.5, 500 mM NaCl and 20
414 mM imidazole. Flow through containing OtsA was collected, concentrated and loaded to
415 a Superdex 200 column equilibrated with 20 mM TRIS pH 7.5, 500 mM NaCl. Fraction
416 purity was determined by SDS-page and purest fractions were pooled concentrated to ~10
417 mg.ml⁻¹ in 20 mM TRIS pH 7.5 350 mM NaCl, flash frozen in liquid nitrogen and stored
418 at -80 °C. The same purification protocol was used for all *MtrOtsA* mutants.

419

420 **Crystallization and data collection**

421 *MtrOtsA* crystallization screens and optimization were performed at 18 °C using sitting-
422 drop vapour diffusion method. 300 nl of pure OtsA at 10 mg.ml⁻¹ was mixed in 1:1 ratio
423 with well solution using a Phoenix robot (Art Robbins). Initial conditions were obtained

424 in classics suite crystallization screen (Qiagen), solution 36. Crystals obtained in this
425 condition diffracted only up to 3 Å. Therefore, further optimization was performed using
426 the additive screen HT (Hampton Research) and ethylene glycol was found to be the best
427 additive. The final optimized condition consisted of 0.7 M sodium potassium tartrate, 0.1
428 M CHES pH 10 and 10% v/v ethylene glycol. Crystals appeared after 4 days in this
429 condition. To obtain ligand-bound structures soaking was performed in the optimized
430 condition using the hanging drop vapour diffusion method as follows: 1 µl of protein
431 storage buffer containing 5 mM of ligand was mixed with 1 µl of reservoir solution and
432 drops were left to equilibrate against 500 µl of reservoir solution for 3 days. Crystals were
433 then transferred to the pre-equilibrated drops and incubated for 24h. A cryogenic solution
434 was prepared by adding ethylene glycol up to 25% v/v to mother liquor. Crystals were
435 briefly transferred to this solution, flash frozen in liquid nitrogen and stored for data
436 collection. To obtain an ADP-G6P-OtsA ternary complex co-crystallization with 5mM
437 ADP and G6P was performed instead, as all attempts to soak G6P alone or G6P in the
438 presence of ADP have failed. Crystals were obtained in the Wizard Classic I&II screen
439 (Rigaku), solution E10 and were flash frozen in liquid nitrogen after a brief soak in a
440 solution containing mother liquor and 25% ethylene glycol. The same condition was used
441 to obtain ADP:F6P:OtsA complex.

442 All data sets were collected at stations I04, I04-1 and I24 at Diamond Light Source
443 (Oxford, UK). Data collection and refinement statistics are summarized in (Table S1).

444

445 **Structure solution and refinement**

446 Diffraction data were processed and reduced using MOSFLM (53) and Aimless (54) from
447 the CCP4 suite (55), or autoPROC from Global Phasing Limited (56). The apo form
448 crystallized in I4₁22 space group with one protomer per asymmetric unit. ADP-G6P-OtsA

449 ternary complex crystallized in P6₂22 space group again with one protomer per
450 asymmetric unit.

451 Initial phases were determined with PHASER (57) from PHENIX software package (58)
452 using the structure of *E. coli* OtsA (PDB entry 1UQU) (31) as a search model. Model
453 building was done with Coot (59) and refinement was performed in PHENIX (58).
454 Structure validation was performed using Coot and PHENIX tools (58, 59). All the figures
455 were prepared with Pymol (<http://www.pymol.org>).

456

457 **Prediction of mutations in ligand affinity**

458 To provide an insight on which residues to mutate, we used mCSM-lig a software that
459 predicts the effect of mutations in ligand affinity (37) on the X-ray crystal structure of
460 OtsA with ADP-glucose (5JIO).

461

462 **Enzymatic Assays**

463 Formation of T6P was assessed by a continuous colorimetric assay that followed the
464 release of NDP by measuring the oxidation of NADH at 340nm, in the presence of
465 pyruvate kinase and lactate dehydrogenase. All reagents used were obtained from Sigma-
466 Aldrich. The enzymatic reactions (200 μ l) were performed at 37 °C and contained 50 mM
467 TRIS pH 7.5, 200 mM NaCl, 10 mM MgCl₂, 50 mM KCl, 0.3 mM NADH, 2.5 mM
468 phosphoenolpyruvate (PEP), 10 units of pyruvate kinase/lactate dehydrogenase, 0.1 μ M
469 enzyme and varying concentrations of G6P and NDP-glucose to determine kinetic
470 parameters.

471 The effect of trehalose and T6P as feedback inhibitors, and G1P, F6P, F16BP, CHES,
472 2PG, 3PG, cAMP and 2OG as allosteric regulators, was tested in the conditions described
473 above but with fixed concentrations of G6P and ADP-glucose (both 0.3 mM). The same

474 conditions were used to test possible allosteric regulators for wild type OtsA and mutants
475 Arg213Glu and Arg384Glu. All experiments were performed in triplicate in a PheraStar
476 plate reader (BMG Labtech) and data was analysed with Prism 5 (Graphpad Software).
477 To assess the inhibitory effect of ADP and allosteric effect of phosphoenolpyruvate an
478 end-point assay was performed instead. Reactions (100 μ l) containing 50 mM TRIS pH
479 7.5, 200 mM NaCl, 10 mM MgCl₂, 50 mM KCl, 4 μ M *Mtr*OtsA, 0.3 mM ADP-glucose,
480 0.3 mM G6P and varying concentrations of ADP and PEP were incubated at 37 °C and
481 stopped at different time points with 10 μ l of 1 M HCl, incubated for 1 minute and
482 neutralized with NaOH. The reactions were diluted with 100 μ l acetonitrile and run at 25
483 °C on a Waters I-class UHPLC with a PDA detector (258 nm) using a ACQUITY UHPLC
484 BEH Amide column (2.1 x 100 mm, 1.7 μ m). Gradient elution (delivered at 0.13 mL/min)
485 was employed using 80/20 acrilamide/water with 0.1 % NH₂OH (A) and water with 0.1
486 % NH₂OH (B) which started at 90 % A and decreased linearly to 55 % A over 10 min.

487

488 **Isothermal Titration Calorimetry**

489 Binding interaction between OtsA and ligands was characterized at 25 °C, using a
490 Microcal ITC200 titration calorimeter (Microcal). OtsA concentration of 60 μ M was used
491 for all titrations. Ligands (1 mM) were injected in 2 μ l aliquots. Titration data was
492 recorded in 20mM TRIS pH 7.5, 500mM NaCl. Data was analysed by fitting a simple
493 single-site model using Origin software (Microcal).

494

495

496

497

498

499

500

501

502 **References**

503

- 504 1. Nobre A, Alarico S, Maranhã A, Mendes V, & Empadinhas N (2014) The molecular biology
505 of mycobacterial trehalose in the quest for advanced tuberculosis therapies.
506 *Microbiology* 160(Pt 8):1547-1570.
- 507 2. Iturriaga G, Suarez R, & Nova-Franco B (2009) Trehalose metabolism: from
508 osmoprotection to signaling. *Int J Mol Sci* 10(9):3793-3810.
- 509 3. Webb KM & DiRuggiero J (2012) Role of Mn²⁺ and compatible solutes in the radiation
510 resistance of thermophilic bacteria and archaea. *Archaea* 2012:845756.
- 511 4. Singer MA & Lindquist S (1998) Thermotolerance in *Saccharomyces cerevisiae*: the Yin
512 and Yang of trehalose. *Trends Biotechnol* 16(11):460-468.
- 513 5. Lu H, *et al.* (2011) Lack of trehalose accelerates H₂O₂-induced *Candida albicans*
514 apoptosis through regulating Ca²⁺ signaling pathway and caspase activity. *PLoS ONE*
515 6(1):e15808.
- 516 6. Lee J, *et al.* (2013) Trehalose Glycopolymers as Excipients for Protein Stabilization.
517 *Biomacromolecules* 14(8):2561-2569.
- 518 7. Kandror O, DeLeon A, & Goldberg AL (2002) Trehalose synthesis is induced upon
519 exposure of *Escherichia coli* to cold and is essential for viability at low temperatures.
520 *Proceedings of the National Academy of Sciences of the United States of America*
521 99(15):9727-9732.
- 522 8. Cardoso FS, Castro RF, Borges N, & Santos H (2007) Biochemical and genetic
523 characterization of the pathways for trehalose metabolism in *Propionibacterium*
524 *freudenreichii*, and their role in stress response. *Microbiology* 153(Pt 1):270-280.
- 525 9. Tapia H & Koshland DE (2014) Trehalose is a versatile and long-lived chaperone for
526 desiccation tolerance. *Current biology : CB* 24(23):2758-2766.
- 527 10. Thevelein JM (1984) Regulation of trehalose mobilization in fungi. *Microbiol Rev*
528 48(1):42-59.
- 529 11. Elbein AD (1974) The metabolism of alpha, alpha-trehalose. *Advances in carbohydrate*
530 *chemistry and biochemistry* 30:227-256.
- 531 12. Elbein AD, Pan YT, Pastuszak I, & Carroll D (2003) New insights on trehalose: a
532 multifunctional molecule. *Glycobiology* 13(4):17R-27R.
- 533 13. Djonovic S, *et al.* (2013) Trehalose biosynthesis promotes *Pseudomonas aeruginosa*
534 pathogenicity in plants. *PLoS Pathog* 9(3):e1003217.
- 535 14. Wahl V, *et al.* (2013) Regulation of flowering by trehalose-6-phosphate signaling in
536 *Arabidopsis thaliana*. *Science* 339(6120):704-707.
- 537 15. O'Hara LE, Paul MJ, & Winkler A (2013) How do sugars regulate plant growth and
538 development? New insight into the role of trehalose-6-phosphate. *Molecular plant*
539 6(2):261-274.
- 540 16. Paul MJ, Primavesi LF, Jhurrea D, & Zhang Y (2008) Trehalose metabolism and signaling.
541 *Annu Rev Plant Biol* 59:417-441.
- 542 17. Fraenkel D & Nielsen J (2016) Trehalose-6-phosphate synthase and stabilization of yeast
543 glycolysis. *FEMS Yeast Res* 16(1):fov100.

- 544 18. Deroover S, Ghillebert R, Broeckx T, Winderickx J, & Rolland F (2016) Trehalose-6-
545 phosphate synthesis controls yeast gluconeogenesis downstream and independent of
546 SNF1. *FEMS Yeast Res* 16(4).
- 547 19. Williams B, *et al.* (2015) Trehalose Accumulation Triggers Autophagy during Plant
548 Desiccation. *PLoS genetics* 11(12):e1005705.
- 549 20. Rubinsztein DC, Bento CF, & Deretic V (2015) Therapeutic targeting of autophagy in
550 neurodegenerative and infectious diseases. *J Exp Med* 212(7):979-990.
- 551 21. Boot M, *et al.* (2017) Cell envelope stress in mycobacteria is regulated by the novel signal
552 transduction ATPase IniR in response to trehalose. *PLoS genetics* 13(12):e1007131.
- 553 22. Avonce N, Mendoza-Vargas A, Morett E, & Iturriaga G (2006) Insights on the evolution
554 of trehalose biosynthesis. *BMC Evol Biol* 6:109.
- 555 23. Zaparty M, *et al.* (2013) The first prokaryotic trehalose synthase complex identified in
556 the hyperthermophilic crenarchaeon *Thermoproteus tenax*. *PLoS ONE* 8(4):e61354.
- 557 24. Murphy HN, *et al.* (2005) The OtsAB pathway is essential for trehalose biosynthesis in
558 *Mycobacterium tuberculosis*. *J Biol Chem* 280(15):14524-14529.
- 559 25. Korte J, *et al.* (2016) Trehalose-6-Phosphate-Mediated Toxicity Determines Essentiality
560 of OtsB2 in *Mycobacterium tuberculosis* In Vitro and in Mice. *PLoS Pathog*
561 12(12):e1006043.
- 562 26. Errey JC, *et al.* (2010) Mechanistic insight into enzymatic glycosyl transfer with retention
563 of configuration through analysis of glycomimetic inhibitors. *Angew Chem Int Ed Engl*
564 49(7):1234-1237.
- 565 27. Gibson RP, Turkenburg JP, Charnock SJ, Lloyd R, & Davies GJ (2002) Insights into
566 trehalose synthesis provided by the structure of the retaining glucosyltransferase OtsA.
567 *Chem Biol* 9(12):1337-1346.
- 568 28. Miao Y, *et al.* (2017) Structural and In Vivo Studies on Trehalose-6-Phosphate Synthase
569 from Pathogenic Fungi Provide Insights into Its Catalytic Mechanism, Biological
570 Necessity, and Potential for Novel Antifungal Drug Design. *MBio* 8(4).
- 571 29. Asencion Diez MD, *et al.* (2017) The Production and Utilization of GDP-glucose in the
572 Biosynthesis of Trehalose 6-Phosphate by *Streptomyces venezuelae*. *J Biol Chem*
573 292(3):945-954.
- 574 30. Jiang Y, *et al.* (2010) The catalytic efficiency of trehalose-6-phosphate synthase is
575 effected by the N-loop at low temperatures. *Arch Microbiol* 192(11):937-943.
- 576 31. Gibson RP, Tarling CA, Roberts S, Withers SG, & Davies GJ (2004) The donor subsite of
577 trehalose-6-phosphate synthase: binary complexes with UDP-glucose and UDP-2-deoxy-
578 2-fluoro-glucose at 2 Å resolution. *J Biol Chem* 279(3):1950-1955.
- 579 32. Pan YT, Carroll JD, & Elbein AD (2002) Trehalose-phosphate synthase of *Mycobacterium*
580 *tuberculosis*. Cloning, expression and properties of the recombinant enzyme. *Eur J*
581 *Biochem* 269(24):6091-6100.
- 582 33. Chen X, *et al.* (2017) A trehalose biosynthetic enzyme doubles as an osmotic stress
583 sensor to regulate bacterial morphogenesis. *PLoS genetics* 13(10):e1007062.
- 584 34. Asencion Diez MD, *et al.* (2015) Allosteric regulation of the partitioning of glucose-1-
585 phosphate between glycogen and trehalose biosynthesis in *Mycobacterium*
586 *tuberculosis*. *Biochim Biophys Acta* 1850(1):13-21.
- 587 35. Killick KA (1979) Trehalose 6-phosphate synthase from *Dictyostelium discoideum*:
588 partial purification and characterization of the enzyme from young sorocarps. *Arch*
589 *Biochem Biophys* 196(1):121-133.
- 590 36. Silva Z, Alarico S, & da Costa MS (2005) Trehalose biosynthesis in *Thermus thermophilus*
591 RQ-1: biochemical properties of the trehalose-6-phosphate synthase and trehalose-6-
592 phosphate phosphatase. *Extremophiles* 9(1):29-36.
- 593 37. Pires DE, Blundell TL, & Ascher DB (2016) mCSM-lig: quantifying the effects of mutations
594 on protein-small molecule affinity in genetic disease and emergence of drug resistance.
595 *Sci Rep* 6:29575.

- 596 38. Londesborough J & Vuorio OE (1993) Purification of trehalose synthase from baker's
597 yeast. Its temperature-dependent activation by fructose 6-phosphate and inhibition by
598 phosphate. *Eur J Biochem* 216(3):841-848.
- 599 39. Hu P, *et al.* (2009) Global functional atlas of Escherichia coli encompassing previously
600 uncharacterized proteins. *PLoS biology* 7(4):e96.
- 601 40. Huergo LF & Dixon R (2015) The Emergence of 2-Oxoglutarate as a Master Regulator
602 Metabolite. *Microbiol Mol Biol Rev* 79(4):419-435.
- 603 41. Zheng L, *et al.* (2012) Structural and functional analysis of validoxylamine A 7¹-phosphate
604 synthase ValL involved in validamycin A biosynthesis. *PLoS ONE* 7(2):e32033.
- 605 42. Cavalier MC, *et al.* (2012) Mechanistic Insights into Validoxylamine A 7¹-Phosphate
606 Synthesis by VldE Using the Structure of the Entire Product Complex. *PLoS ONE* 7(9).
- 607 43. Chandra G, Chater KF, & Bornemann S (2011) Unexpected and widespread connections
608 between bacterial glycogen and trehalose metabolism. *Microbiology* 157(Pt 6):1565-
609 1572.
- 610 44. Trevisol ET, Panek AD, De Mesquita JF, & Eleutherio EC (2014) Regulation of the yeast
611 trehalose-synthase complex by cyclic AMP-dependent phosphorylation. *Biochim*
612 *Biophys Acta* 1840(6):1646-1650.
- 613 45. Sengupta S, *et al.* (2014) Purification, characterization, sequencing and molecular
614 cloning of a novel cysteine methyltransferase that regulates trehalose-6-phosphate
615 synthase from *Saccharomyces cerevisiae*. *Biochim Biophys Acta* 1840(6):1861-1871.
- 616 46. Potel CM, Lin MH, Heck AJR, & Lemeer S (2018) Widespread bacterial protein histidine
617 phosphorylation revealed by mass spectrometry-based proteomics. *Nat Methods*
618 15(3):187-190.
- 619 47. Bennett BD, *et al.* (2009) Absolute metabolite concentrations and implied enzyme active
620 site occupancy in Escherichia coli. *Nat Chem Biol* 5(8):593-599.
- 621 48. Albe KR, Butler MH, & Wright BE (1990) Cellular concentrations of enzymes and their
622 substrates. *J Theor Biol* 143(2):163-195.
- 623 49. Sharma S, Jadli M, Singh A, Arora K, & Malhotra P (2014) A secretory multifunctional
624 serine protease, DegP of *Plasmodium falciparum*, plays an important role in thermo-
625 oxidative stress, parasite growth and development. *FEBS J* 281(6):1679-1699.
- 626 50. Murashko ON & Lin-Chao S (2017) Escherichia coli responds to environmental changes
627 using enolase degradosomes and stabilized DicF sRNA to alter cellular morphology. *Proc*
628 *Natl Acad Sci U S A* 114(38):E8025-E8034.
- 629 51. Morita T, Kawamoto H, Mizota T, Inada T, & Aiba H (2004) Enolase in the RNA
630 degradosome plays a crucial role in the rapid decay of glucose transporter mRNA in the
631 response to phosphosugar stress in Escherichia coli. *Mol Microbiol* 54(4):1063-1075.
- 632 52. Bornemann S (2016) alpha-Glucan biosynthesis and the GlgE pathway in *Mycobacterium*
633 *tuberculosis*. *Biochem Soc Trans* 44(1):68-73.
- 634 53. Leslie AGW & Powell HR (2007) Processing diffraction data with MOSFLM. *Nato Sci Ser*
635 *li Math* 245:41-51.
- 636 54. Evans PR & Murshudov GN (2013) How good are my data and what is the resolution?
637 *Acta Crystallogr D* 69:1204-1214.
- 638 55. Winn MD, *et al.* (2011) Overview of the CCP4 suite and current developments. *Acta*
639 *Crystallogr D Biol Crystallogr* 67(Pt 4):235-242.
- 640 56. Vonrhein C, *et al.* (2011) Data processing and analysis with the autoPROC toolbox. *Acta*
641 *Crystallogr D Biol Crystallogr* 67(Pt 4):293-302.
- 642 57. McCoy AJ, *et al.* (2007) Phaser crystallographic software. *Journal of applied*
643 *crystallography* 40(Pt 4):658-674.
- 644 58. Adams PD, *et al.* (2010) PHENIX: a comprehensive Python-based system for
645 macromolecular structure solution. *Acta Crystallogr D Biol Crystallogr* 66(Pt 2):213-221.
- 646 59. Emsley P, Lohkamp B, Scott WG, & Cowtan K (2010) Features and development of Coot.
647 *Acta Crystallogr D Biol Crystallogr* 66(Pt 4):486-501.

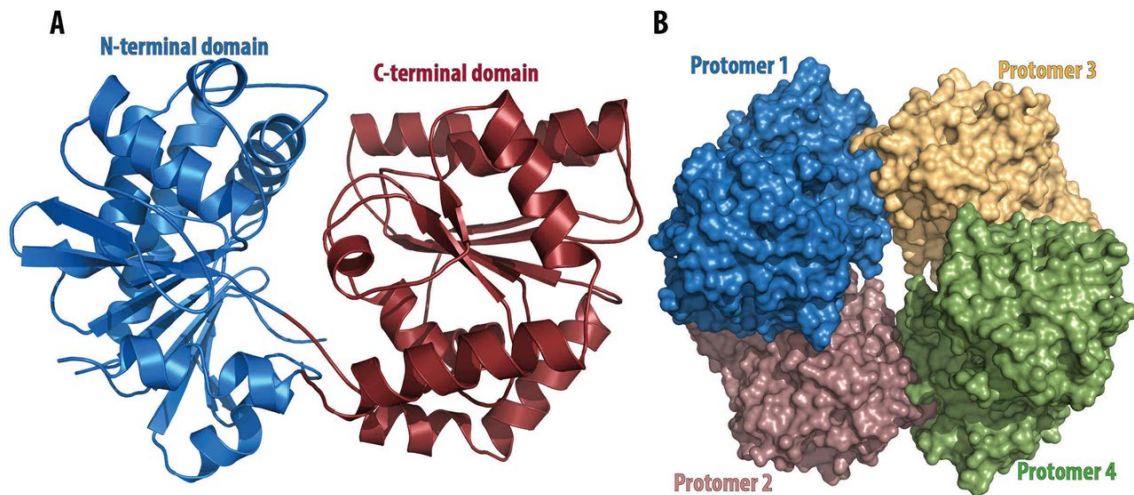
648 60. Jubb HC, *et al.* (2017) Arpeggio: A Web Server for Calculating and Visualising Interatomic
649 Interactions in Protein Structures. *J Mol Biol* 429(3):365-371.

650

651

652 **Figures**

653



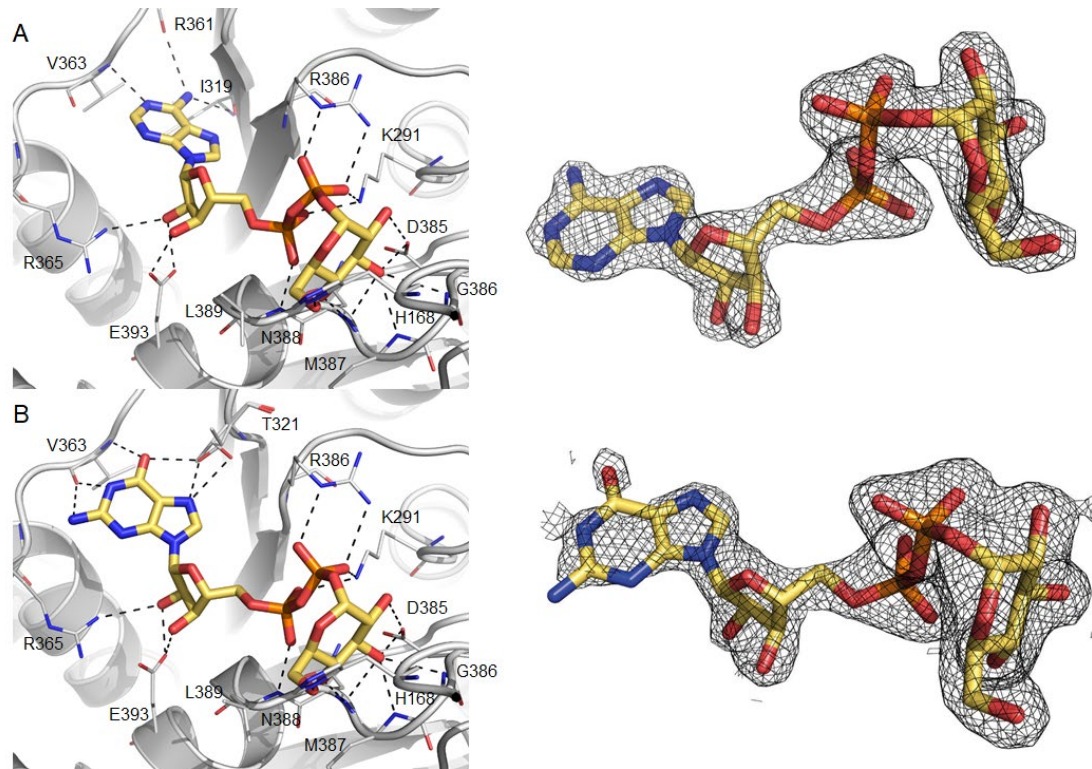
654

655 **Figure 1:** (A) Representation of the overall structure of *M. thermoresistibile* OtsA. The
656 N-terminal domain consists of residues 1-247 and 462-486, the C-terminal domain of
657 residues 248-461. View of *M. thermoresistibile* OtsA tetramer (B).

658

659

660



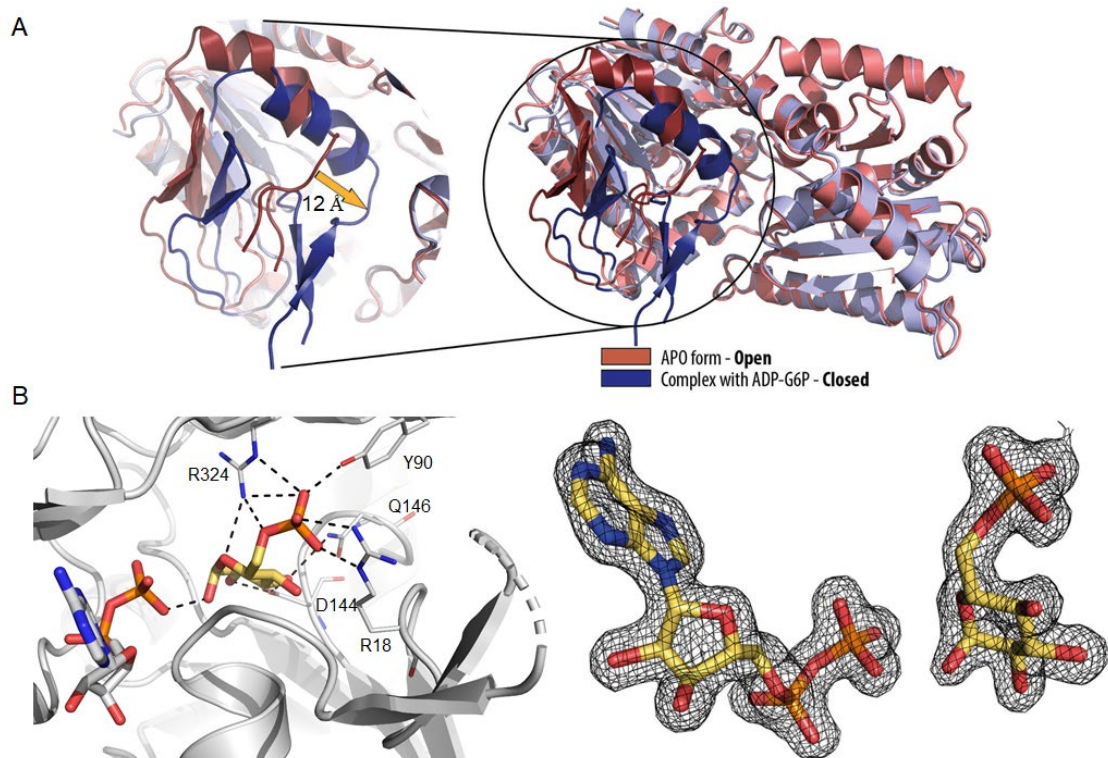
661

662 **Figure 2:** Detailed view of the active site of *M. thermoresistibile* OtsA with ADP-glucose

663 (A) and with GDP-glucose bound (B) with “omit maps” shown. Black dashed lines

664 represent hydrogen bonds.

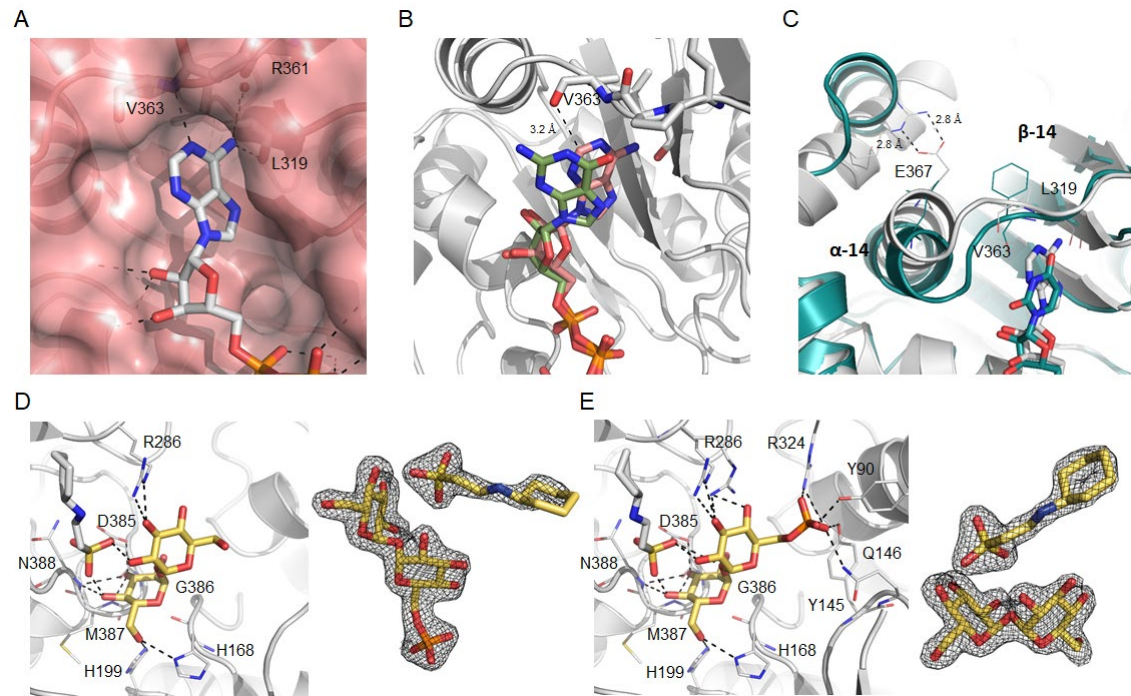
665



666

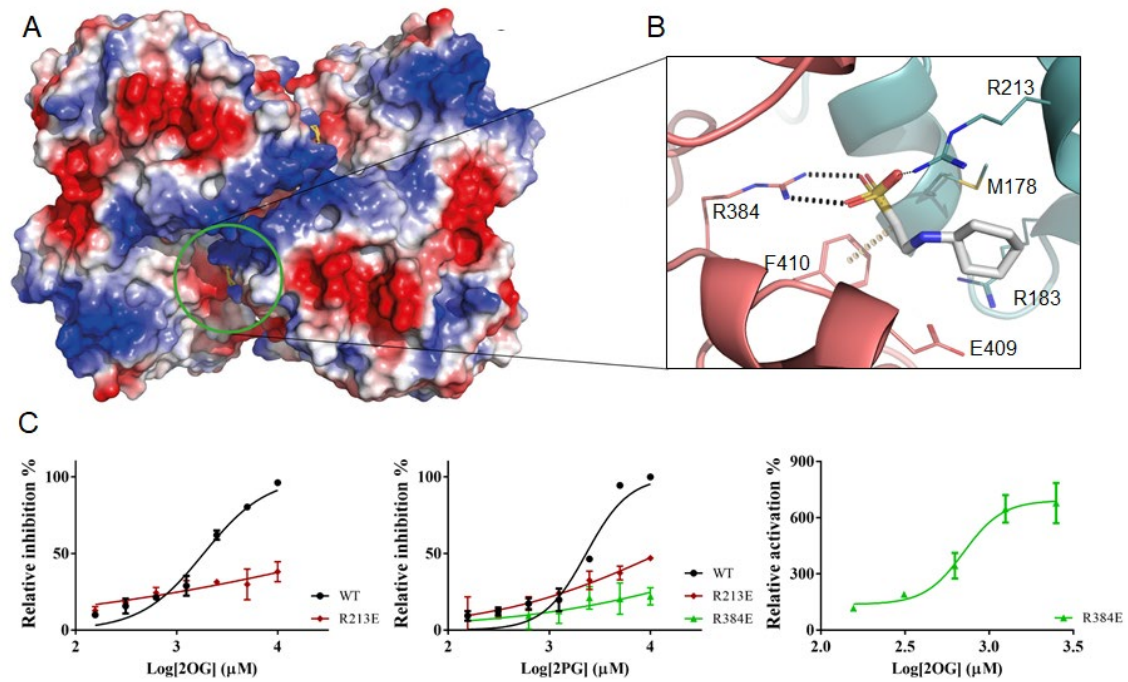
667 **Figure 3:** View of OtsA in an open (salmon and red) and closed conformation (violet and
668 blue) and superposition of the two conformations. (B) Representation of the active site of
669 *M. thermoresistibile* OtsA with ADP (white) and G6P (yellow) bound with “omit map”
670 shown. Black dashed lines represent hydrogen bonds.

671



673 **Figure 4:** View of the binding site of the adenine moiety of ADP-glucose (A).
674 Superposition of ADP-glucose and GDP-glucose structures (B). Superposition of
675 *MtrOtsA* structure with ADP-glucose bound and *E. coli OtsA* structure with UDP-glucose
676 bound (PDB code: 1UQU) (C). Alpha helix 14 (α -14) and beta strand 14 (β -14) are
677 shown. Detailed view of the active site of *M. thermoresistibile* OtsA with trehalose (D)
678 and with T6P bound (E) with CHES visible in both structures. “Omit maps” are shown
679 both trehalose, T6P and CHES. Black dashed lines represent hydrogen bonds.

680



681

682 **Figure 5:** View of the allosteric site of *M. thermoresistibile* OtsA with CHES bound with

683 protein surface electrostatic potential shown (A). Detailed view of the CHES binding site

684 and its interactions with OtsA (B). The interactions were calculated with Arpeggio (60)

685 using the apo structure (5JIJ). Black dots represent hydrogen bonds and yellow disks a

686 carbon- π interaction. The two protomers are colored differently. (C) Activity profiles of

687 *M. thermoresistibile* wild type OtsA and the allosteric site mutants Arg213Glu and

688 Arg384Glu in the presence of the allosteric effectors 2OG and 2PG.

689

690

691

692

693

694

695

696

697 **Table 1:** Kinetic parameters of *M. thermoresistibile* OtsA.

698

	Substrate	K_m (mM)	k_{cat} (s ⁻¹)	k_{cat}/K_m
WT	ADP-Glucose	0.25 ± 0.02	26 ± 1	104 ± 13
	GDP-Glucose	0.29 ± 0.02	5.1 ± 0.2	18 ± 2
	UDP-Glucose	1.7 ± 0.1	36 ± 1	21 ± 2
	Glucose-6P	3.3 ± 0.1	26 ± 1	7.9 ± 0.5
L319I	ADP-Glucose	0.71 ± 0.18	8.4 ± 0.7	12 ± 2
	GDP-Glucose	0.35 ± 0.04	3.1 ± 0.1	8.9 ± 1.4
	UDP-Glucose	1.4 ± 0.1	8.9 ± 0.4	6.4 ± 0.7
	Glucose-6P	3.3 ± 0.2	6.4 ± 0.2	1.9 ± 0.2
V363F	ADP-Glucose	0.60 ± 0.03	11 ± 1	18 ± 2
	GDP-Glucose	0.74 ± 0.08	14 ± 1	19 ± 3
	UDP-Glucose	0.68 ± 0.06	13 ± 1	19 ± 3
	Glucose-6P	3.1 ± 0.2	19 ± 1	6.1 ± 0.7
L319I, E367L	ADP-Glucose	0.63 ± 0.04	14 ± 1	22 ± 3
	GDP-Glucose	0.70 ± 0.05	9.2 ± 0.4	13 ± 2
	UDP-Glucose	0.63 ± 0.03	15 ± 1	24 ± 3
	Glucose-6P	3.7 ± 0.2	21 ± 1	5.7 ± 0.5
L319I, V363F, E367L	ADP-Glucose	1.3 ± 0.1	19 ± 1	15 ± 2
	GDP-Glucose	0.90 ± 0.06	16 ± 1	18 ± 2
	UDP-Glucose	0.52 ± 0.05	22 ± 1	42 ± 6
	Glucose-6P	3.2 ± 0.2	17 ± 1	5.3 ± 0.6
R213E	ADP-Glucose	0.31 ± 0.01	56 ± 2	180 ± 13
	Glucose-6P	3.3 ± 0.3	33 ± 2	10 ± 1
R384E	ADP-Glucose	1.9 ± 0.2	3.2 ± 0.1	1.7 ± 0.2
	Glucose-6P	2.9 ± 0.2	2.1 ± 0.2	0.77 ± 0.05

699

700

701 **Table 2:** Effect of allosteric regulators in *M. thermoresistibile* OtsA activity. Values are
702 in (mM) and 95% confidence intervals are given in brackets.

	WT	R213E	R384E
2OG	IC ₅₀ = 1.8 (1.6-2.1)	IC ₅₀ = 73 (18-302)	EC ₅₀ = 0.70 (0.56-0.88)
	IC ₅₀ = 2.3 (2.0-2.7)	IC ₅₀ = 12 (6.3-24)	IC ₅₀ < 100

703